Development of a refined illumination and reflectance approach for optimal construction site interior image enhancement

Abstract:

Purpose - Images taken from construction site interiors often suffer from low illumination and poor natural colors, which restricts their application for high-level site management purposes. The state-of-the-art low-light image enhancement (LIME) method provides promising image enhancement results. However, they generally require a longer execution time to complete the enhancement. This study aims to develop a refined image enhancement approach to improve execution efficiency and performance accuracy.

Design/methodology/approach - To develop the refined illumination enhancement algorithm named enhanced illumination quality (EIQ), a quadratic expression was first added to the initial illumination map. Subsequently, an adjusted weight matrix was added to improve the smoothness of the illumination map. A coordinated descent optimization algorithm was then applied to minimise the processing time. Gamma correction was also applied to further enhance the illumination map. Finally, a frame comparing and averaging method was used to identify interior site progress.

Findings - The proposed refined approach took around 4.36 to 4.52 seconds to achieve the expected results while outperforming the current LIME method. EIQ demonstrated a lower *lightness-order-error* (*LOE*) and provided higher object resolution in enhanced images. EIQ also has a higher *structural similarity index* (*SSIM*) and *peak-signal-to-noise ratio* (*PSNR*), which indicated better image reconstruction performance.

Originality - The proposed approach provides an alternative to shorten the execution time, improve equalization of the illumination map and provide a better image reconstruction. The approach could be applied to low-light video enhancement tasks and other dark or poor jobsite images for object detection processes.

Keywords: Enhanced image quality; Low-light image enhancement; Indoor; Photogrammetry; Illumination map; Construction site

1. Introduction

Delayed interior works in construction projects have bottleneck effects on succeeding activities such as the impact on the overall project completion, cost overruns (Gurevich and Sacks, 2014) and ineffective work-in-progress management while resulting in further schedule delay (Omar and Nehdi, 2016). Timely evaluation of interior construction works based on reliable sources (site data or information) is essential, which not only can minimize disputes over completed works, but also generates precise information for project control and management (Golparvar-Fard *et al.*, 2016; Memarzadeh *et al.,* 2013). The advancement in photogrammetry and computer vision techniques in the past two decades have provided a unique opportunity to apply high-precision approaches to capturing and assessing the site images for construction progress monitoring (Fard and Peña-Mora, 2007; Zhang et al., 2009, Omar and Nehdi, 2016; Alizadehsalehi and Yitmen, 2019; Kopsida *et al.,* 2015). However, the interior construction environment often encounters practical issues related to lighting conditions (low illumination, fluctuating lighting levels) and the sensitivity of the region-of-interest (ROI), which makes the application of indoor photogrammetry more challenging than outdoors to assess the progress (Lukins and Trucco, 2007; Fathi and Brilakis, 2012; Hamledari et al., 2017; Golparvar-Fard et al., 2019; Borin and Cavazzini, 2019; Deng et al., 2020; Xue et al., 2021). Reducing or removing occluding noise and blocking objects from interior images can be challenging due to poor and dim lighting in indoor locations. The captured objects under such conditions are often difficult to perceive using current vision-based techniques (Franco-Duran and Guillermo, 2016). Site images having poor visual quality could affect the robustness and accuracy of high-level tasks (image segmentation, object detection) (Franco-Duran and Guillermo, 2016; Kropp *et al.,* 2017; Kropp *et al.,* 2016).

The current research on the application of photogrammetry in the construction discipline has paid less attention to improving fundamental tasks such as low-light image enhancement (LIME) (Ekanayake et al., 2021). Image enhancement involves image processing techniques to highlight key information, eliminate some secondary information and improve the quality of identification. Also, the processing technique must ensure that the images are at a high-quality level required for visual recognition systems (Guo *et al.,* 2017; Oneata *et al.*, 2014). Illumination map smoothing is one of the most effective ways to enhance the illumination of low-light images. The classic image enhancement algorithm LIME method (Guo et al., 2017) utilizes an efficient mathematical model to smooth the illumination map. Even though it has demonstrated prominent image enhancement performance in recent years, there are still limitations in terms of execution efficiency and accuracy metrics. Ren *et al.* (2018) and Li *et al.* (2018) adopted the classic LIME mathematical model to increase the performance of low-light images. However, these developments significantly increased the running time. The recognition and detection of objects in construction projects must be done in a short time. Therefore, this paper intended to develop a refined approach to efficiently reconstruct and enhance low-light images taken from interior construction environments. It was also envisioned to reduce image processing time, and achieve an optimal balance between illumination and reflectance without losing the readability as well as details for the use of construction monitoring and coordination purposes. A mathematical modification to LIME, named enhanced illumination quality (EIQ) was developed to obtain an optimally equalized illumination map during the reconstruction of the images. The proposed approach employed the coordinate descent method to solve the developed mathematical model and reduce the computation time. The gamma correction technique was also added as a supplementary step to prevent overexposure in the reconstructed images. The combination of EIQ, coordinate descent method and gamma correction brings novelty to image enhancement and provides high-quality images with higher efficiency and accuracy. It also provides an opportunity to develop efficient object detection and indoor progress tracking in the dark construction site.

2. Literature Review

2.1 Background

With the availability of affordable high-resolution digital surveillance cameras and accessories along with having enhanced bandwidth capacity, the capturing and sharing of a large number of construction images has been facilitated (Lu and Lee, 2017; Golparvar-Fard *et al.,* 2015). Digital cameras have been used in construction sites primarily for security and marketing purposes. Their application has been extended for verifying the progress and other project management purposes because of its cost-effective and easy-to-use aspect (Fini et al., 2021). However, imaging technologies require a favourable environment and rely on good illuminance. The significant light difference in a single frame, especially when captured from an indoor environment, is a key concern, which could result in images possibly containing both highly bright and very dark areas at the same time. This affects the resolution of images while significantly degrading the performance of algorithms that are primarily designed for high-quality image data. The frames captured from surveillance cameras often require pre-processing before becoming valuable and distinguishable data.

Lighting conditions in dynamic construction job sites, particularly interior environments, are often affected by back-lights, shadows and artificial light sources, which makes the application of photogrammetry challenging (Kropp et al., 2013; Kropp et al., 2014; Vincke et al., 2019; Ekanayake et al., 2021). Images taken in the low-light area suffer from low visibility, low contrast and high-level noise (Li et al., 2018). The backlight primarily generated by the external natural lighting entering the site causes different exposure and strong light gradient in site images, which constrain feature extraction (Kropp et al., 2013). Raising the camera's gain setting and enhancing the amplification of the signal from the camera sensor are often adopted to capture sufficiently bright images of a dark scene. However, this could add more noise to the image. Increasing the capturing time is another conventional approach to enhance the brightness of the image, although this can result in motion blur if the camera does not perfectly stand still. The contrast in dark areas is considered another challenge in the application of photogrammetry in interior construction environments. The images often suffer from problems of under-or over-exposure, depicting the overlap between dark and bright areas.

Adopting and modifying visual recognition algorithms for each lighting condition (Hamledari *et al.*, 2017; Franco-Duran and Guillermo, 2016) and removing image noise (e.g., temporary moving objects) (Brilakis *et al.*, 2010; Wu, 2011) are still major challenges encountered in pre-processing dark images in congested interior construction sites. For example, Deng *et al.* (2020) demonstrated that images taken in low resolution or under poor light conditions were unsuitable for classifier training and in the development of an automated progress monitoring model for tiling works in construction projects. Fathi and Brilakis (2012) pointed out that poor lighting conditions are a major barrier to obtaining consistent image analysis in photography while having few common features among multiple images. During the development of the 4D augmented reality model for automating construction progress, Golparvar-Fard *et al.* (2019) also found that poor illumination in the construction site environments makes it difficult to perform consistent analysis of the imagery. Borin and Cavazzini (2019) assessed the condition of the reinforced concrete bridges with a combined machine learning approach (BIM and photogrammetry) and found that photos of damaged concrete taken in low-light conditions were undetectable. In addition, during the development of an advanced image-based 3D reconstruction method for construction progress monitoring, Xue *et al.* (2021) found that the intensity of light and shadows had a significant impact on image quality. Poor lighting results in blurry images that are unsuitable for high-level tasks such as progress monitoring. Therefore, recent research suggested that addressing low visibility, high-level noise and low contrast in low-light images is critical

2.2 Low-light image enhancement (LIME) technique

To address general image enhancement challenges, Guo *et al.* (2017) proposed the LIME technique to improve images taken in low-lighting conditions (Guo *et al.,* 2017). LIME is based on the Retinex theory (Land, 1977), which divides images into two pixel-wise components (reflectance and illumination). Its goal is to improve the visual quality of photos by brightening and enhancing as well as displaying details that are kept out of sight in the darkness. In summary, LIME (Loh *et al*., 2019) helps to develop statistical modelling and distribution of low-light image intensities as well as high-frequency coefficients for enhancing the contrast and brightness of the photos (Huang *et al.,* 2013; Łoza *et al.,* 2013). LIME also provides a transformation model that employs parameterized functions to carry out the transformation mapping of images from dim- to bright-light spaces while preserving contextual information (Wu, 2011; Fu *et al.,* 2012; Li *et al*., 2020). LIME smoothest out the illumination map through a mathematical model. According to Retinex theory (Land, 1977), images can be divided into two factors, i.e., reflection and illumination (Figure 1).

$$\boldsymbol{L} = \boldsymbol{T} \circ \boldsymbol{R} \qquad \textbf{(1)}$$

where L and R are the captured image and the desired recovery, respectively. T represents the illumination map and the operator '○' refers to element-wise multiplication.

According to the Retinex theory, the LIME method estimates an illumination map to enhance low-light images. LIME accomplishes this by first estimating the initial illumination map and then smoothing it to enhance image visual quality. Generally, LIME considers the following assumptions to estimate the illumination map:

1) The estimated illumination map (T) does not differ much from the initial illumination map $(\hat{T})$ (to maintain image illumination).
2) In an estimated illumination map (T), the value for each pixel should be as close as possible to the neighbor pixels (to enhance image quality and smoothness).

Although minimizing the difference between illumination values of neighbor pixels could improve the visual quality in an estimated illumination map (T), a big difference between the illumination value of each pixel and its corresponding value in $\hat{T}$ might make the image very dark. Therefore, the LIME approach attempted to balance the two above-mentioned issues to enhance illumination while maintaining image readability. Accordingly, LIME uses the following mathematical model to estimate the illumination map.

$$\min_{\boldsymbol{T}} \|\hat{\boldsymbol{T}} - \boldsymbol{T}\|_{\boldsymbol{F}}^{2} + \boldsymbol{\alpha}\|\boldsymbol{W} \circ \nabla \boldsymbol{T}\|_{1} \tag{2}$$

where α is a coefficient which balances the involved two terms and $\|\hat{T} - T\|_F$ and $\|W \circ \nabla T\|_1$ represent Frobenius and $l_1$norms, respectively. W is the weight matrix and ∇T is the first-order derivative filter, which only contains $\nabla_h T$(horizontal) and $\nabla_v T$(vertical). $\hat{T}$ represents the initial illumination map. LIME uses the following relation to estimate the initial illumination map ($\hat{T}$) (Figure 1).

$$\hat{\boldsymbol{T}}(\boldsymbol{x}) \leftarrow \max_{c \in \{\boldsymbol{R},\boldsymbol{G},\boldsymbol{B}\}} \boldsymbol{L}^{c}(\boldsymbol{x}) \tag{3}$$

where R, G, and B represent the intensity of light in the red, green, and blue channels, respectively. In the objective function (Eq. 2), the first phrase aims to preserve the initial illumination map ($\hat{T}$) while the second phrase aims to make it smoother. In other words, the first phrase guarantees the brightness and the second phrase guarantees the visual quality of enhanced images.

Despite these achievements, the current LIME approach has a few limitations related to the hand-crafted manipulations on the illumination map, the involvement of various parameter tuning tasks and over-enhancement, which affects the performance and execution efficiency (Li *et al.,* 2020; Li *et al.,* 2018; Ren *et al.,* 2018). A deficiency of LIME is attributable to the phrase $\|W \circ \nabla T\|_1$ as it is not differentiable. This issue significantly increases the computation time because the optimal point in non-smooth models is irregular. For example, Ren et al. (2018) developed a joint LIME and denoising model via decomposition in a successive image sequence, with the goal of simultaneously enhancing low illumination images and removing inherent noise issues. Li *et al.* (2018) proposed a robust Retinex model that explicitly predicted the noise map out of the robust Retinex model while simultaneously estimating a structure-revealed reflectance map and a piece-wise smoothed illumination map. However, the model developed by *Li et al.* took a longer running time to complete the image enhancement (Li *et al.*, 2018). In addition, LIME traditionally has limitations in considering the illumination factor, which could result in some information being lost while processing low-light images. It is noteworthy to highlight that the Retinex theory is not adopted for estimating illumination.

To overcome the issue abovementioned, an option is to convert this phrase into a quadratic phrase. There are a number of simple and fast methods for solving quadratic models, including

Newton's method (Coleman and Li, 1996) and the coordinate descent method (Hildreth, 1957). For this reason, LIME uses Eq. (4) to approximate the phrase $||W \circ \nabla T||_1$ to a quadratic phrase.

$$||\boldsymbol{W} \circ \boldsymbol{\nabla T}||_1 = \lim_{\varepsilon \to 0^+} \left(\sum_{x} \sum_{d \in \{v,h\}} \frac{\boldsymbol{W_d(x)(\nabla_d T(x))^2}}{|\boldsymbol{\nabla_d T(x)}| + \boldsymbol{\varepsilon}} \right) \tag{4}$$

As a result, the approximation of Eq (2) can be written as:

$$\min_{\boldsymbol{T}} \left\|\boldsymbol{\hat{T}} - \boldsymbol{T}\right\|_F^2 + \boldsymbol{\alpha} \left(\sum_{x} \sum_{d \in \{v,h\}} \frac{\boldsymbol{W_d(x)(\nabla_d T(x))^2}}{|\boldsymbol{\nabla_d T(x)}| + \boldsymbol{\varepsilon}} \right) \tag{5}$$

This approximation can have a negative effect on the smoothness of the illumination map (T). In this study, we proposed to add another quadratic expression to Eq (5) to improve the lost smoothness while addressing the shortcoming. We also proposed to provide a better approximation of the phrase $||W \circ \nabla T||_1$ by reduce the number of calculations. Finally, a coordinate descent method was added to reduce the processing time of the proposed model.

A better approximation of Eq (5) was proposed to reduce the computational volume. By considering $\frac{1}{|\nabla_d T(x)|+\varepsilon}$ as a constant value and integrating it into α ($\boldsymbol{\alpha'} \leftarrow \alpha \frac{1}{|\nabla_d T(x)|+\varepsilon}$), the Eq (5) can be converted to the following quadratic equation:

$$\min_{\boldsymbol{T}} \left\|\boldsymbol{\hat{T}} - \boldsymbol{T}\right\|_F^2 + \boldsymbol{\alpha}' \left(\sum_{x} \sum_{d \in \{v,h\}} \boldsymbol{W_d(x)(\nabla_d T(x))^2} \right) \tag{6}$$

In practice, the value of $\frac{1}{|\nabla_d T(x)|+\varepsilon}$ for different images are approximately equal to 100. Therefore, it is suggested that the $\boldsymbol{\alpha'}$ value in Eq (6) be approximately 100 times the α value in Eq (5).

The weight matrix is another factor that affects the computation time of image enhancement. Guo et al. (2017) proposed a weighting strategy in which every element of matrix W equates to one. This strategy reduces the computation time of the model. Using this strategy, Eq (6) can be rewritten as follows:

$$\min_{\boldsymbol{T}} \left\|\boldsymbol{\hat{T}} - \boldsymbol{T}\right\|_F^2 + \boldsymbol{\alpha} \left(\sum_{x} \sum_{d \in \{v,h\}} \boldsymbol{(\nabla_d T(x))^2} \right) \tag{7}$$

The reduction to quadratic form and the adoption of a simple strategy for the weight matrix in Eq (7) can have negative effect on the smoothness of the illumination map (T).

2.3 Gamma correction and background subtraction

Gamma correction is another critical element of preprocessing, in which a picture decoding technique is applied to establish the relationship between the numerical value of a pixel and its real luminance (Bull, 2014). The value of gamma (γ) is usually determined experimentally by achieving a calibration performance through the imaging system with a full spectrum of established luminance values (Chang and Reid, 1996). Often the imaging device does not have direct access to such calibration. Many commercially available digital cameras adopt different gamma values. However, the process does not always ensure the linearity of the photos taken (Bull, 2014). Therefore, eliminating these nonlinearities before successive image processing would be beneficial (Farid, 2001). Gamma correction can be used to reduce the light effect by altering the pixel value. These preprocessing techniques can improve feature extraction, point matching and subsequent vision measurement (Xu *et al.,* 2009). We further applied a simple but effective gamma correction technique to the proposed model to ensure that the achieved equalization of the illumination map does not lead to overexposure in some of the reconstructed images. This assisted in precisely capturing the luminance variation. Even though many digital cameras available in the market dynamically adjust the gamma values, this does not necessarily lead to an optimal luminance. Hence, further calibration of the images is needed. That is particularly applicable to the time-lapse cameras which are mounted in an indoor site environment.

Images taken in interior construction settings are generally shot in extremely low light with limited illumination and therefore, these images are subjected to noise (Li *et al.*, 2020). Frequently changing scenes such as congested interior construction sites further accelerate the problem of noise in the images. Static or moving site operatives, machines, equipment and tools all contribute to the noise. Therefore, another important consideration in the preprocessing of on-site images is identifying moving foreground objects and distinguishing them from the non-moving background.

A background subtraction technique, named frame differencing (FD) has been developed to help identify illumination, motion and geometry background changes in the images (Kartika and Mohamed, 2011). After a camera is mounted at the designated location to capture the view, a background model is determined by collecting the dominant pixel values from the frames. To detect the moving objects in the frames, the foreground objects are identified by finding the pixel value discrepancies between existing frames and the background model exceeding a threshold (Park and Brilakis, 2012a). Background subtraction can be used to detect all objects in motion regardless of their appearance. FD has been employed in several studies to detect moving objects in exterior construction environments. It has also been experimented as the part of two post-processing techniques, including adaptive threshold and shadow detection in hue, saturation and value (HSV) color space for exterior environments (Kartika and Mohamed, 2011). For example, Park and Brilakis (2012b) identified and localized site operatives in video frames by incorporating various methods, including background subtraction, the histogram of oriented gradients (HOG) and the HSV color histogram (Park and Brilakis, 2012). A variety of cues, including motion, shape, and color were adopted to reduce the detection regions for moving objects (e.g., humans and equipment) on site. Park *et al.* (2012) also applied a similar approach in tracking equipment by detecting and identifying each equipment entity. Memarzadeh *et al.* (2013) proposed a combined HOGs and hue–saturation colors for automated 2D recognition of workers and equipment from site videos. The experimental results showed that FD in combination with such techniques can distinguish moving objects in exterior construction environments from other static objects with no shadow (Memarzadeh *et al.,* 2013). Both the gradient orientations and hue–saturation colors were established. The results were combined and depicted on the HOG + C Descriptors. These applications illustrate the effectiveness of FD for on-site tracking purposes in an exterior construction environment. However, changes associated with dynamic scenes, such as shadows, illumination and in-camera/digital noise could lead to a lower object detection accuracy. Given the above insight, FD will be applied in this study to examine the effectiveness of the image enhancement hybrid approach for the LIME task. In this paper, we attempted to ameliorate the execution speed and optimize the accuracy of the illumination map. The model refinement started with the use of an initial illumination map, the brightness values of adjacent pixels as well as the average initial illumination map. The approach resulted in a more equalized illumination map by developing the refined LIME approach named EIQ. The details of our approach will be elaborated in the next section.

3. Methodology

The proposed refined LIME approach, named EIQ, is presented in this section. First, the framework of the proposed method is presented, followed by the development of the refined LIME model. Subsequently, the experiment settings of the proposed approach are presented.

3.1. Framework overview

Following the state-of-the-art LIME approach based on the traditional Retinex theory developed by Guo *et al.* (2017), we implemented the proposed method by first estimating the initial illumination map for the input low light colour image $\boldsymbol{L}$. In order to reduce the computational time, this phrase was converted into a quadratic phrase by adding a quadratic expression. Subsequently, an adjusted weight matrix was generated to improve the smoothing of the initial illumination map ($\hat{T}$). To minimise the processing time, the initial illumination map ($\hat{T}$) was further refined by adding a coordinate descent optimization algorithm. To achieve the equalization of the illumination map while having no overexposure in the reconstructed image at the same time, gamma correction was applied to enhance the illumination map T^{γ}. The input variables in this process include the initial illumination map ($\hat{T}$), whereas the output variables include the estimated illumination map (T) and an enhanced (R) (Figure 1). Next, a heat map was developed by a cumulative sum of the light differences between contiguous frames. It helps understand the magnitude of changes in lighting levels to interior site images in this experiment. Then, a comparing and averaging method was applied to identify the progress of the raised floor installation from the frames.

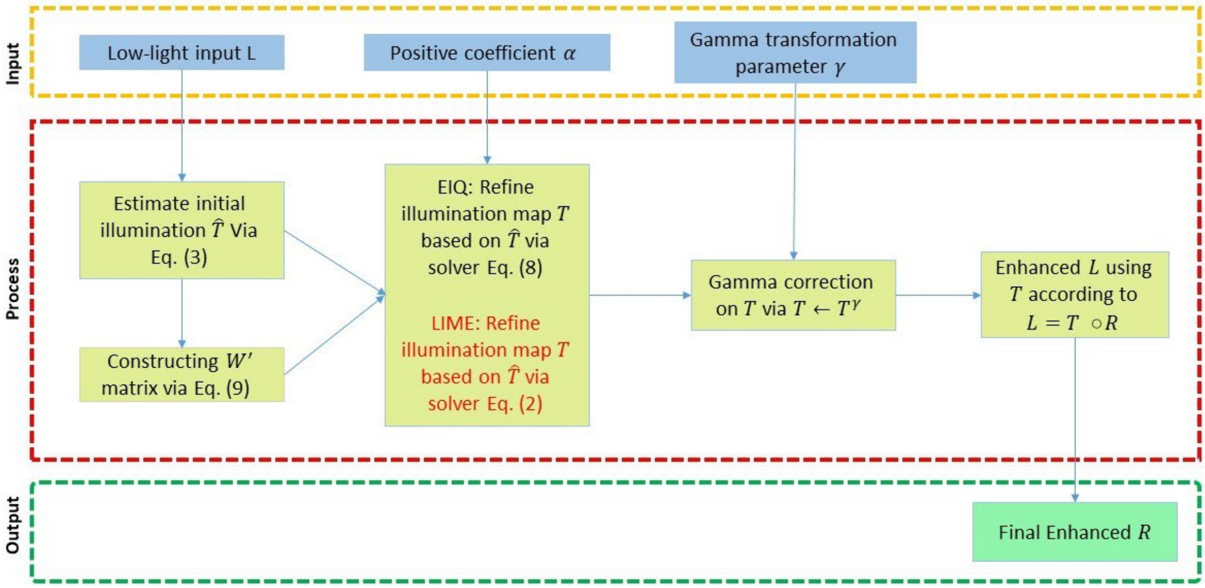

Figure 1: Steps to enhance illumination of low-light images

3.2. Introducing mathematical adjustments to optimise illumination map

To increase the smoothness of the illumination map (T), the quadratic phrase $\beta\|W' \times (T - M)\|_F^2$ was first added to Eq (7).

$$\min_T f(T) = \left\|\hat{T} - T\right\|_F^2 + \alpha\left(\sum_x \sum_{d\in\{v,h\}} \nabla_d T(x)^2\right) + \beta\|W' \times (T - M \times O)\|_F^2 \quad \textbf{(8)}$$

where M is equal to the average values of the initial illumination map ($\hat{T}$), O is a matrix whose elements are all equal to one, and β represents the equilibrium coefficient between the terms. W' in Eq (8) is called the adjusted weight matrix, which can be obtained from Eq (9).

$$W' = \frac{1}{\left\|\hat{T} - M \times O\right\|_1 + \epsilon} \quad \textbf{(9)}$$

The phrase $\beta\|W' \times (T - M \times O)\|_F^2$ in Eq (8) brings the illumination map (T) values closer to the average of the initial illumination map ($\hat{T}$). This can improve the smoothing of the illumination map compared to the LIME model (Eq 5). Therefore, this phrase can improve the uniformity of the illumination map (T). By adding this phrase to the model, the approximation error used in the proposed model can be reduced.

The main advantages of Eq (8) compared to Eq (2) (i.e. the state-of-the-art LIME discussed in previous section) are differentiability and quadratic stability, which makes the adjusted model more accurate and faster. In addition, Eq (8) is an unrestricted and convex model and thus, simple methods can be used to solve it. In order to reduce the processing time, a coordinate descent (CD) method was proposed to quickly solve the proposed mathematical model (Eq 8). The coordinate descent (CD) method is a classic iterative method for solving optimization problems (Hildreth, 1957). It is closely related to the Gauss-Seidel and Jacobi methods for solving a linear system. Depending on the nature of the problem, a number of variables are considered as parameters in each iteration of the CD method and the problem is then solved using these values. This idea reduces the size of the problem. Compared to a full-update method, such as the gradient descent and Newton's method, the coordinate update is simpler and more efficient. The CD method also has lower memory requirements (Rahmani *et al.,* 2009). Therefore, the CD method and its variants, such as coordinate gradient descent, have become popular for solving large-scale problems under both convex and non-convex settings (Rahmani *et al.*, 2009; Elad *et al.*, 2007; Hong *et al.*, 2017; Wright, 2015). As mentioned below, a method based on CD can be formulated according to the nature of the proposed mathematical model (Eq 8).

First, Eq (8) can be rewritten as follows:

$$\min_{\boldsymbol{T}} \sum_{i=1}^{m}\sum_{j=1}^{n} \boldsymbol{f(T)} = \left(\boldsymbol{T(i,j)} - \widehat{\boldsymbol{T}}\boldsymbol{(i,j)}\right)^2 + \boldsymbol{\beta W'(i,j)} \times (\boldsymbol{T(i,j)} - \boldsymbol{M}))^2$$
$$+ \ \boldsymbol{\alpha} \sum_{i=2}^{m-1}\sum_{j=2}^{n-1} (\boldsymbol{T(i,j)} - \boldsymbol{T(i-1,j)})^2 + (\boldsymbol{T(i,j)} - \boldsymbol{T(i+1,j)})^2 + (\boldsymbol{T(i,j)}$$
$$- \boldsymbol{T(i,j-1)})^2 + (\boldsymbol{T(i,j)} - \boldsymbol{T(i,j+1)}^2$$

(10)

If the optimal solution of the other variables of Eq (10) can be obtained except $T(i,j)$, then $T(i,j)$ remains as the only variable of relation Eq (10). As a result, the Eq (10) relation can be written as follows:

$$\min_{\boldsymbol{T(i,j)}} \boldsymbol{g(T(i,j)} = \left(\boldsymbol{T(i,j)} - \widehat{\boldsymbol{T}}\boldsymbol{(i,j)}\right)^2 + \boldsymbol{\beta(W'(i,j)}$$
$$\times (\boldsymbol{T(i,j)} - \boldsymbol{M}))^2 + \ (\boldsymbol{T(i,j)} - \boldsymbol{T(i-1,j)})^2$$
$$+ (\boldsymbol{T(i,j)} - \boldsymbol{T(i+1,j)}))^2 + (\boldsymbol{T(i,j)}$$
$$- \boldsymbol{T(i,j-1)})^2 + (\boldsymbol{T(i,j)} - \boldsymbol{T(i,j+1)}^2 + \boldsymbol{C}$$

(11)

where C represents a fixed value. Eq (11) is a quadratic univariate optimization problem. Therefore, using Eq (11), the optimal solution $T(i,j)$ can be easily obtained. Therefore, the second differentiable of Eq (11) was first calculated as follows:

$$\boldsymbol{g''(T(i,j)} = \boldsymbol{2\beta W^{'}(i,j)} + \boldsymbol{10} \geq \boldsymbol{0} \qquad \textbf{(12)}$$

The second derivative of Eq (11) is positive. Hence, the first derivative at the optimal point is equal to zero. Therefore, the optimal solution *T(I,j)* was obtained from the following linear and univariate equation:

$$\boldsymbol{g'(T(i,j)} = \boldsymbol{2(T(i,j)} - \widehat{\boldsymbol{T}}\boldsymbol{(i,j)}) + \boldsymbol{2\beta W'(i,j)} \times (\boldsymbol{T(i,j)} - \boldsymbol{M}) + \ \boldsymbol{2(T(i,j)}$$
$$- \boldsymbol{T(i-1,j)} + \boldsymbol{2(T(i,j)} - \boldsymbol{T(i+1,j)} + \boldsymbol{2(T(i,j)}$$
$$- \boldsymbol{T(i,j-1)}) + \boldsymbol{2(T(i,j)} - \boldsymbol{T(i.j+1)} = \boldsymbol{0}$$

(13)

By solving Eq (13), the optimal solution $T(i,j)$ can be obtained as:

$$\boldsymbol{T(i,j)} = \frac{\boldsymbol{2\beta W'(i,j)M + 2\alpha(\widehat{T}(i,j) + T(i-1,j) + T(i+1,j) + T(i,j-1) + T(i,j+1))}}{\boldsymbol{2 + 2\beta W'(i,j) + 8\alpha}} \quad \textbf{(14)}$$

As seen in Eq (14), it is easy to find the optimal value $T(i,j)$ if the other values of the illumination map are known. This supports the notion of using a CD optimization algorithm to solve model (8). The *EIQ* algorithm developed in this paper was intended to iteratively solve the objective function presented by Eq (8) while using the above notion. The first component of the objective function (8) for $T = \widehat{T}$ is equal to zero. In addition, for $T = \widehat{T}$ the other two components of Eq (8) are also relatively small. Therefore, *EIQ* uses $\widehat{T}$ as a starting point. If T^{t-1} can be obtained from the repetition of $t-1$, then T^t must be calculated from Eq (17) and $T^t(i,j)$ for *i* and *j*. For the values of $T(i-1,j)$, $T(i+1,j)$, $T(i,j-1)$ and $T(i,j+1)$ in Eq (15), the solution obtained from the previous iteration (T^{t-1}) was utilized. Therefore, $T^t(i,j)$ was obtained from the following equation:

$$\boldsymbol{T^t(i,j)} = \frac{\boldsymbol{2\beta W'(i,j)M + 2\alpha(\widehat{T}(i,j) + T^{t-1}(i-1,j) + T^{t-1}(i+1,j) + T^{t-1}(i,j-1) + T^{t-1}(i,j+1))}}{\boldsymbol{2 + 2\beta W'(i,j) + 8\alpha}} \quad \textbf{(15)}$$

Before calculating $T^t(i,j)$ values, the $T^t(i-1,j)$ and $T^t(i,j-1)$ were also calculated. To accelerate the convergence process, it is suggested that in Eq (16), $T^t(i-1,j)$ and $T^t(i,j-1)$ should be used instead of $T^{t-1}(i-1,j)$ and $T^{t-1}(i,j-1)$. The proposed algorithm for calculating the value of $T^t(i,j)$ uses the following equation:

$$\boldsymbol{T^t(i,j)} = \frac{\boldsymbol{2\beta W'(i,j)M + 2\alpha(\widehat{T}(i,j) + T^{t-1}(i-1,j) + T^{t-1}(i+1,j) + T^{t-1}(i,j-1) + T^{t-1}(i,j+1))}}{\boldsymbol{2 + 2\beta W'(i,j) + 8\alpha}} \quad \textbf{(16)}$$

- *EIQ stop condition:* The EIQ can continue until $|f(T^t) - f(T^{t-1})| < \epsilon$. However, verifying this condition in any algorithm iteration can be time-consuming. On the other hand, high accuracy is not required to enhance low-light images while using Eq (8).
- *Computational complexity of the EIQ:* The computational complexity of EIQ is related to step 5. In step 5, the calculation of $T^t(i,j)$ is in the order of $O(1)$. The number of $T^t(i,j)$ calculated in this step is equal to $n \times m$. Therefore, the computational complexity of step 5 is equal to $O(nm)$. Given that the number of iterations of the algorithm is equal to t, the computational complexity of the whole algorithm is equal to $O(tnm)$. Therefore, EIQ is a polynomial algorithm for solving mathematical model (8).

- *Convergence of the EIQ:* Suppose the solution generated by EIQ is $T^0, T^1, T^2, \ldots, T^t$. According to the calculation of $T^t(i,j)$, the $f(T^0), f(T^1), f(T^2), \ldots, f(T^t)$ sequence will follow a decreasing trend. On the other hand, $f(T) \geq 0$ for any desired T. The $f(T^0), f(T^1), f(T^2), \ldots, f(T^t)$ sequence will be descending and finite. Therefore, the sequence will be convergent. As a result, we can obtain:

$$\exists \boldsymbol{N}\ \forall\ \boldsymbol{t} \geq \boldsymbol{N}\ \left|\boldsymbol{f}(\boldsymbol{T}^{t+1}) - \boldsymbol{f}(\boldsymbol{T}^{t})\right| < \boldsymbol{\epsilon} \qquad \textbf{(17)}$$

From Eq (17) for each *i* and *j*, the following can be concluded:

$$\left|\boldsymbol{f}\left(\boldsymbol{T}^t(\mathbf{1},\mathbf{1}), \ldots, \boldsymbol{T}^{t+1}(\boldsymbol{i},\boldsymbol{j}), \ldots, \boldsymbol{T}^t(\boldsymbol{m},\boldsymbol{n})\right) - \boldsymbol{f}\big(\boldsymbol{T}^t(\mathbf{1},\mathbf{1}), \ldots, \boldsymbol{T}^t(\boldsymbol{i},\boldsymbol{j}), \ldots, \boldsymbol{T}^t(\boldsymbol{m},\boldsymbol{n})\big)\right| \leq \boldsymbol{\epsilon} \qquad \textbf{(18)}$$

By putting $\Delta = T^{t+1}(i,j) - T^t(i,j)$ it can be concluded that:

$$\left|\boldsymbol{f}\big(\boldsymbol{T}^t(\mathbf{1},\mathbf{1}), \ldots, \boldsymbol{T}^t(\boldsymbol{i},\boldsymbol{j}) + \Delta, \ldots, \boldsymbol{T}^t(\boldsymbol{m},\boldsymbol{n})\big) - \boldsymbol{f}\big(\boldsymbol{T}^t(\mathbf{1},\mathbf{1}), \ldots, \boldsymbol{T}^t(\boldsymbol{i},\boldsymbol{j}), \ldots, \boldsymbol{T}^t(\boldsymbol{m},\boldsymbol{n})\big)\right| \leq \boldsymbol{\epsilon} \qquad \textbf{(19)}$$

So, we can obtain:

$$\lim_{\Delta \to \mathbf{0}} \frac{\boldsymbol{f}\big(\boldsymbol{T}^t(\mathbf{1},\mathbf{1}), \ldots, \boldsymbol{T}^t(\boldsymbol{i},\boldsymbol{j}) + \Delta, \ldots, \boldsymbol{T}^t(\boldsymbol{m},\boldsymbol{n})\big) - \boldsymbol{f}\big(\boldsymbol{T}^t(\mathbf{1},\mathbf{1}), \ldots, \boldsymbol{T}^t(\boldsymbol{i},\boldsymbol{j}), \ldots, \boldsymbol{T}^t(\boldsymbol{m},\boldsymbol{n})\big)}{\Delta} = \mathbf{0} \qquad \textbf{(20)}$$

As a result:

$$\forall \boldsymbol{i},\boldsymbol{j}\ \frac{\partial \boldsymbol{f}(\boldsymbol{T}^t)}{\partial \boldsymbol{T}(\boldsymbol{i},\boldsymbol{j})} = \mathbf{0} \qquad \textbf{(21)}$$

Point T^t is an extremum for the function f. On the other hand,

$$\forall\ \boldsymbol{s} \leq \boldsymbol{t}\ \boldsymbol{f}(\boldsymbol{T}^s) \geq \boldsymbol{f}(\boldsymbol{T}^t) \qquad \textbf{(22)}$$

Therefore, $f(\boldsymbol{T}^t)$ is a minimum of f.

According to the above discussion, the proposed method can significantly enhance the illumination of low-light images.

After estimating the illumination map (*T*) by the EIQ, the gamma correction technique was applied to adjust the illumination and reduce the light variation effect as follows:

$$T \leftarrow T^{\gamma} \quad \textbf{(23)}$$

where γ denotes the gamma code that was adjusted to correct luminance. The value of γ was determined experimentally by passing a calibration target with a full range of luminance values through the imaging system.

The final task was to conduct background subtraction/frame differencing. Two frames (Frame A and Frame B) were compared based on Eq. (24) to determine the absolute difference.

$$\begin{aligned} \mathrm{abs}_{\mathrm{difference(A,B)}} &= \sum_{\mathrm{i}}\sum_{\mathrm{j}} |\mathrm{A(i,j)} - \mathrm{B(i,j)}|\, \mathrm{abs}_{\mathrm{difference(A,B)}} \\ &= \sum_{\mathrm{i}}\sum_{\mathrm{j}} |\mathrm{A(i,j)} - \mathrm{B(i,j)}| \end{aligned} \quad \textbf{(24)}$$

Upon the completion of the comparison, a threshold was applied to produce a binary change in the image.

3.3 Experimental settings and performance evaluation parameters

To evaluate the proposed approach, the refined LIME approach was scrutinized based on indoor construction activity images collected from a data centre construction project. Digital cameras were installed to collect time-lapse data from interior construction sites. The main interior construction activities in this project involved the installation of cold shell spaces into colocations, electrical rooms and uninterruptible power supply rooms. To evaluate the proposed approach, a total of 75 time-lapse images of an internally raised floor installation were collected via a surveillance camera.

The experiments were conducted in MATLAB 2017 on a system having 16 GB RAM and an Intel core i7 processor. The computation time for every frame was around 4 seconds while performing the EIQ and 1.75 seconds for the rest of the process. All of the developed codes are provided as supplementary materials. As the time-lapse interval was large (4 minutes), the overall time was found to be sufficient for the operation.

To evaluate the performance of the proposed modifications on the LIME approach and quantify the effectiveness of the EIQ, three commonly used metrics, including 1) lightness-order-error (*LOE*) (Ying *et al.,* 2017), 2) structural similarity index (*SSIM*) (Wang *et al.,* 2004), and 3) peak-signal-to-noise ratio (*PSNR*) were chosen. They were used to measure i) the computation time, and ii) the content and structural similarity between the enhanced images generated from the proposed EIQ model and the current LIME method. *LOE* was used to evaluate the naturalness preservation. A lower *LOE* indicates better perseverance of the image naturalness after enhancement. In other words, the lower *LOE* the better the resolution of objects in enhanced images. The deviation from the original image was measured using *SSIM* and *PSNR*, with higher *SSIM* and *PSNR* values indicating better image reconstruction performance. High *SSIM* and *PSNR* values mean that less changes are made to original images in the LIME process. Excessive changes to original images can change the properties and dimensions of the objects in enhanced images. Therefore, the higher the *SSIM* and *PSNR*, the better the object identification and detection. In this research, these three metrics are employed to evaluate the model performance.

4. Results and Discussion:

Figure 2 demonstrates the EIQ's enhancement results (Figure 2(b)) of the low-light original image (Figure 2(a)). As shown in the figure, the enhanced image obtained higher brightness and readability. The sum of *T* is shown on the vertical axes. As previously mentioned, the gamma value must be changed to achieve the minimum luminance variation. Gamma correction was required for the low-light images taken on-site as the reflection of the artificial lighting resulted in high luminance variation on the investigated images.

We also compared the proposed EIQ method with the results of the state-of-the-art LIME approach. Five enhanced low-light images (i.e. Images A to E) were randomly selected from our dataset for the performance comparison (Figure 3). The brightness of these images was enhanced by two methods (LIME and EIQ). According to the *LOE* metric, the resolution of objects in enhanced images by EIQ was better than LIME. Also based on *SSIM* and *PSNR* metrics, EIQ applies fewer changes to original images than LIME to increase brightness. Accordingly, the identification and detection of objects in enhanced images by EIQ can be compared to LIME (Figure 3).

In addition to the image enhancement performance, efficiency is also an important factor to measure the performance of an algorithm. Figure 3 illustrates the calculation time performance of the proposed EIQ compared to LIME. The EIQ took 4.36–4.52 seconds to enhance sampled images, whereas LIME took 6.01–6.20 seconds to accomplish the enhancement task. This suggests that EIQ can efficiently improve the quality of images while preserving the natural colors and texture with high contrast. It also requires a shorter running time.

(a) *(b)*

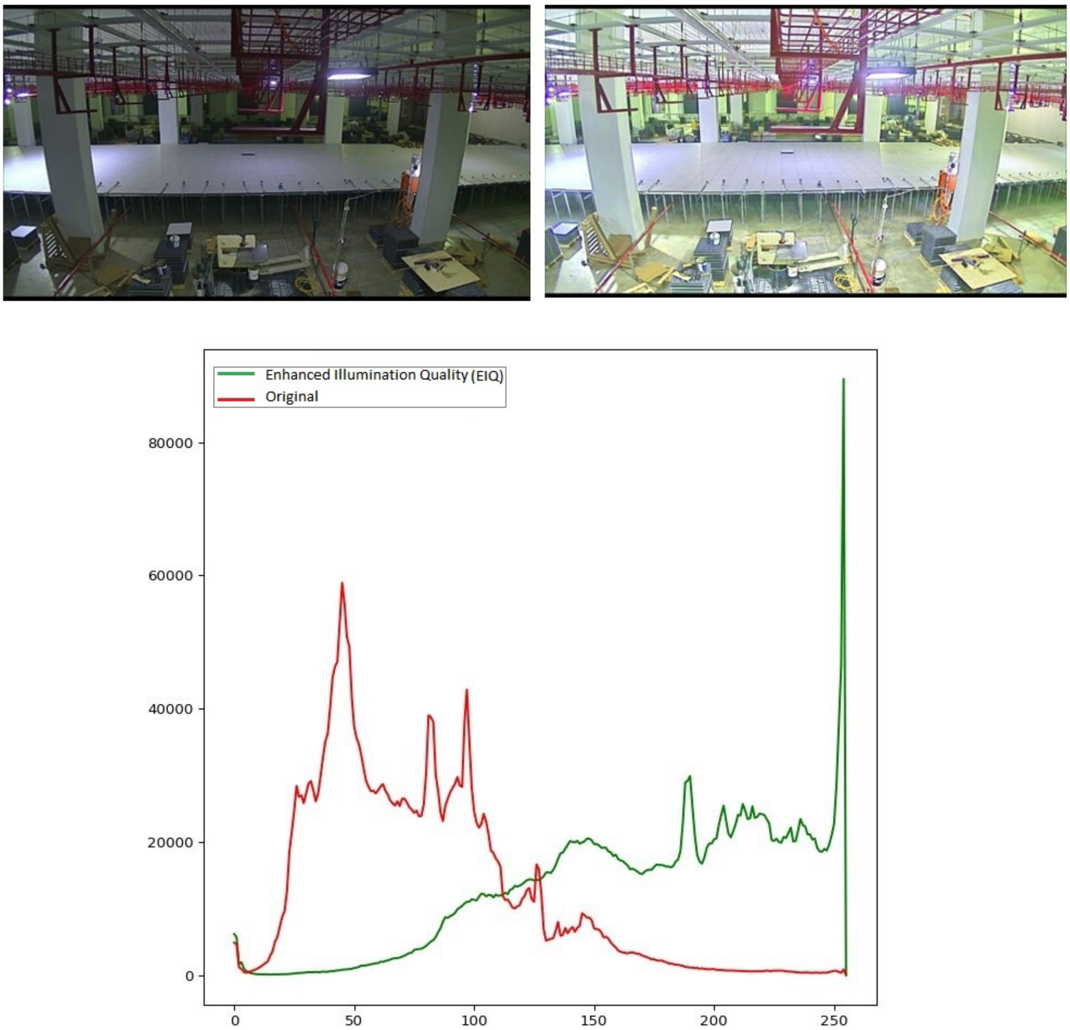

Figure 2: The illumination level of *(a)* original and *(b)* colour enhanced images

	Image A	Image B	Image C	Image D	Image E
Original					
LIME	 LOE: 1,119 SSIM: 0.5227 PSNR: 7.82 Running Time: 6.20	 LOE: 1,104 SSIM: 0.5291 PSNR: 7.90 Running Time: 6.01	 LOE: 1,091 SSIM: 0.5329 PSNR: 7.95 Running Time: 6.14	 LOE: 1,113 SSIM: 0.5433 PSNR: 8.11 Running Time: 6.03	 LOE: 1,155 SSIM: 0.5254 PSNR: 8.02 Running Time: 6.11
EIQ	 LOE: **409** SSIM: **0.5461** PSNR: **8.27** Running Time: **4.51**	 LOE**: 419** SSIM: **0.5531** PSNR: **8.40** Running Time**: 4.50**	 LOE**: 438** SSIM**: 0.5564** PSNR**: 8.45** Running Time: **4.36**	 LOE**: 454** SSIM: **0.5683** PSNR: **8.70** Running Time: **4.43**	 LOE: **437** SSIM: **0.5535** PSNR: **8.69** Running Time: **4.52**

Figure 3: Results of image naturalness, reconstruction performance, and running time of the state-of-the-art LIME and proposed EIQ (refined LIME) methods

In this experiment, a heat map was generated by a cumulative sum of the light differences between adjacent frames to understand the magnitude of lighting level change in interior site images. The map demonstrated that the solar radiation outdoor caused a noticeable light difference between frames of these interior site images over time. The proposed EIQ managed to adjust the illumination and neutralized high variations caused by radiation of a light source or reflection on a glossy material. Figure 4 demonstrated the mechanism of EIQ to calculate the *T* matrix, which represented the difference of light between the sampled original images and the EIQ outputs. As depicted, the amount of enhanced light in a certain area (the fourth column) has an inverse relationship with the amount of original light (the first column) in that area.

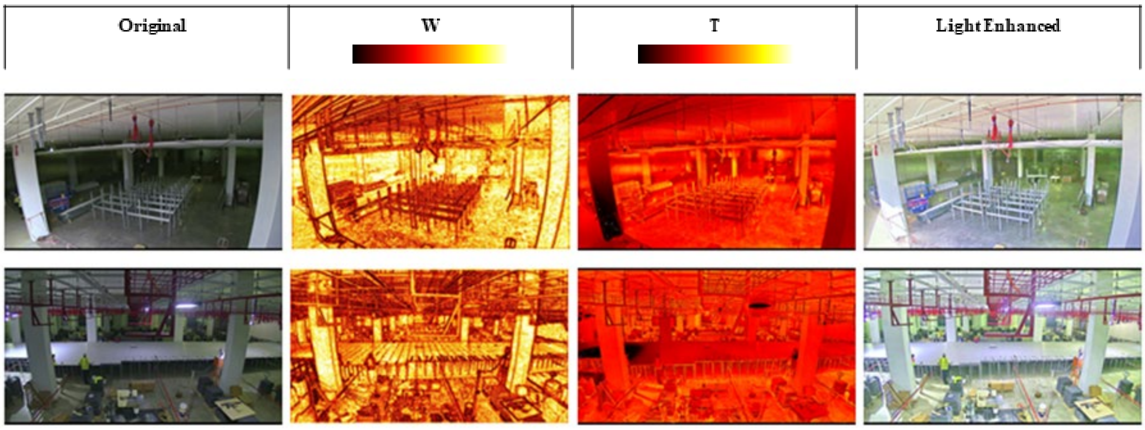

Figure 4: Examples of illumination heat map of *T* and *W* in EIQ

The raised floor panels that were being installed were the objects of interest in this study. Other objects present in a frame that occlude a direct view of the raised floor are considered noise. Such noise should be removed before the post-processing stages. In contrast to the common interest of moving foreground, the objects of interest in this experiment are in the non-moving background, which must be separated from the moving objects present in the foreground. In order to remove the moving foreground objects, rather than using one frame, a sequence of frames was selected from the scene and the average of the frames was adopted to represent the image of the current time. Figure 5 depicts a frame-by-frame comparison and average method for identifying the progress of the raised floor installation. The progress was determined by identifying the difference between the works completed in two consecutive frames, including *f'8* and *f'9*. Frame *f'8* was the average of frame 8 and four neighbor frames before it (i.e., frames *f'4–f'7*), whereas *f'9* was the average of the frame 9 and four neighbor frames after it (i.e., frames *f'10–f'13*). The window size in each batch contained five frames. As the images contain noise that is especially noticeable in a single frame, a sequence of frames was averaged and used in the frame comparison process.

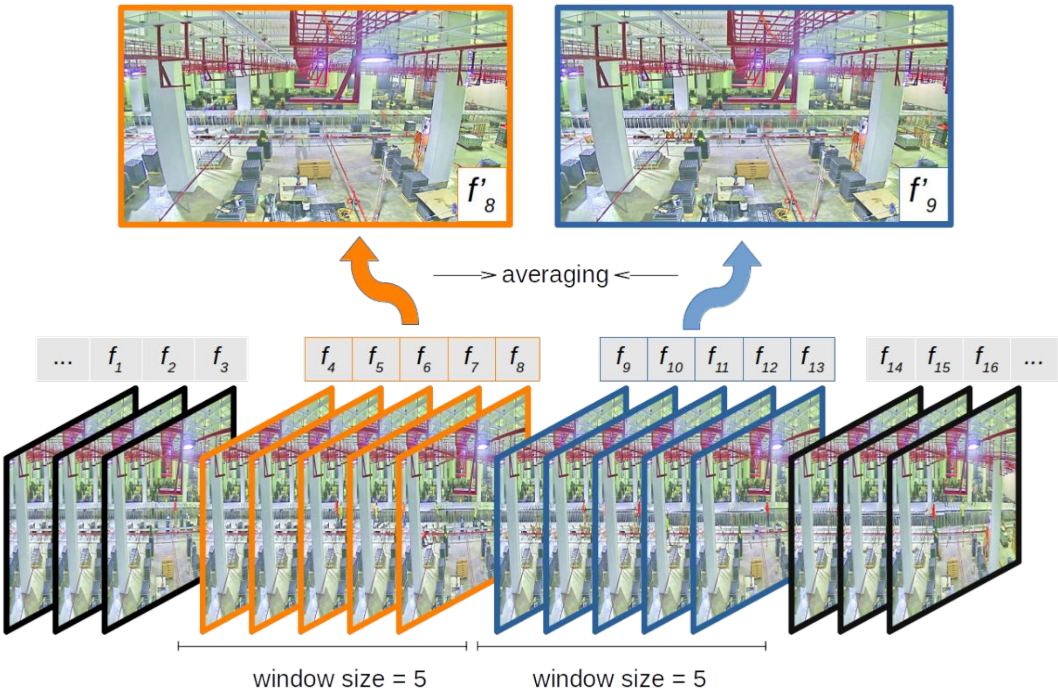

Figure 5: Averaging frames for the raised floor installation progress checking

Rather than using a single frame, a series of frames within a certain time window (e.g., tw=5) should be averaged. Figure 6 illustrates the methods to average a window of frames. The averaging was undertaken by computing an average RGB for each pixel of images across the window of frames. Frames *f'12* and *f'13* represented the average of two consecutive windows of frames, averaging the window of frames having tw=5 while ending at frame *f'12* and starting at *f'13*. These two representative frames were compared to find the progress across the two windows of frames. As shown in Figure 6, a threshold was applied to produce a binary image of changes once the comparison was completed. Progress of construction activities could be presented by drawing contours extracted from the binary image.

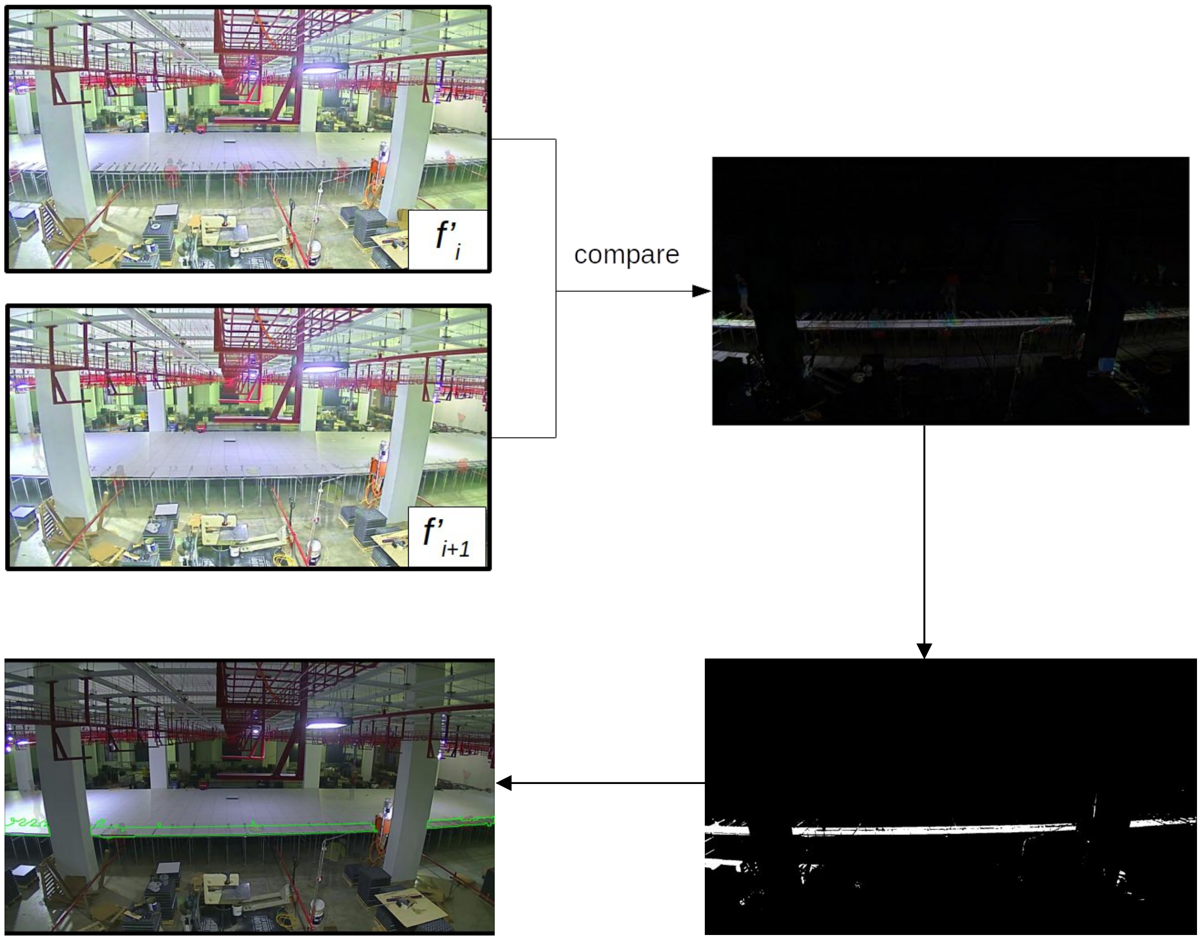

Figure 6: Comparison of the averaged frames and binary images representing the change

With recent advancements, deep learning-based image enhancement methods have shown great potential in image restoration and enhancement. The application of neural networks in enhancing low-light images has particularly received wide attention. Jiang *et al.* (2021) proposed EnlightenGAN, a low illumination enhancement approach based on an unsupervised generative adversarial network (GAN), that can be trained without low/normal-light image pairs. This method minimizes the dependency on paired training data and allows for larger varieties of images to be trained from different domains. Wang *et al.* (2021) proposed LighterGAN, a deep learning and generative adverisal network-based low illumination image enhancement model, which can minimise the image degeneration (insufficient illumination and light pollution) in the unmanned aerial vehicle (UAV). However, this method encountered issues of limited resolution and processing efficiency. Dufaux (2021) argued that technical challenges could remain in the supervised illumination enhancement. The supervised illumination enhancement approach requires a large and fully labelled training dataset and involves a time-consuming as well as expensive process (Dufaux, 2021). The deep learning approach is often vulnerable to adversarial attacks (Dufaux, 2021; Akhtar and Mian, 2018). Therefore, it is difficult to achieve efficient outcomes having low complexity. Saxena and Cao (2021) also reported that the generative adversarial network was difficult to train. Issues such as mode collapse, non-convergence and stability are also common in the GANs training. Dufaux (2021) suggested that combining traditional processing techniques with deep learning models could generate a better outcome by enhancing low complexity solutions and preserving high image enhancement performance at the same time. To improve the accuracy and runtime performance of low-image enhancement, more research should be performed to extend the refined LIME approach and combine it with deep learning methods

5. Conclusions

The temporary lighting in indoor construction environments could result in varying indoor lighting conditions. These variabilities are exacerbated in the images taken from the scene for progress checking purposes. Low-light interior environments strongly affect high-level tasks, such as image segmentation and object detection while hindering the adoption of image processing algorithms for automatic indoor progress monitoring. Despite recent advancements in built-in features for calibrating digital cameras, images from on-site cameras with low illumination often suffer from degradations, such as varying lighting conditions in the presence of shadows, occlusions and highly cluttered scenes, which can result in false ROI detection. This study presented a novel hybrid EIQ algorithm and gamma correction to efficiently stabilize and reconstruct the quality of images collected at an actual indoor construction scene while maintaining an optimal balance between illumination and reflectance without losing the readability.

Low-light images were segmented into scenes using EIQ according to their brightness component similarity. The EIQ offered a solution to expand the illumination of the site images and distinctly enhance image details. The reflection component in the images was further enhanced by gamma correction. The enhanced interior on-site images obtained by the proposed approach enabled the localization of the raised floor panels. The whole process took between 4.36 to 4.52 seconds to achieve the expected results including image enhancement and frame differencing/comparing. In summary, the contributions of this study can be divided into three categories:

- The proposed approach provided a faster (i.e. lower running time) LIME alternative with higher resolution (lower LOE) to improve object identification and detection capability (higher SSIM and PSNR). EIQ was based on modifications made in the LIME mathematical modelling that resulted in improved efficiency (i.e., the average processing time is 27% faster than traditional LIME) and equalization of the illumination map during the reconstruction of images. Overexposure in the reconstructed images was prevented by merging gamma correction into the hybrid algorithm.

- The proposed approach significantly improved the readability of dark construction images and enhanced raw quality images of construction site interiors. It also improved the object detection process for the construction progress monitoring and other on-site cost management tasks such as developing an automated on-site material tracking and counting method to evaluate the work in progress in low-light interior construction environments. The enhanced images could improve safety and security in the dark construction site environment while identifying intruders' faces and reading the license plates. The authors are currently utilizing the enhanced images developed in this study for automatic detection, classification and counting of building materials in a low-light indoor job site environment.
- The proposed method can also be applied to other practical LIME applications in construction and engineering job site environment, including underwater work, sewer inspection and hazy exterior site conditions.

Despite these achievements, one constraint remained that the camera's position had to be known if the identified area within an image was to be aligned with its coordinates and positions in the digital model. The coordinate information of each endpoint of the boundary contour in the studied location and the plane project geometric information of the studied location (i.e., in x and y axes) are required. Low-light image enhancement has great practical significance in computer vision. The experimental results indicated that our approach was quantitatively efficacious and had great potential for low-light video enhancement tasks in interior construction activities and other low-light interior environments. Further research is required to validate the proposed method on various interior site conditions and considers the application of neural networks to enhance low illumination images in construction site.

Acknowledgments

This research was supported by the 5D BIM Lab Research Fund, and the Research Seed Funding Scheme by the Faculty of Design, Architecture and Building, at the University of

Technology Sydney. We thank Biyanka Ekanayake for her assistance with the research background of this study.

References

Akhtar, N., and Mian, A. (2018). “Threat of adversarial attacks on deep learning in computer vision: a survey” *IEEE Access*, Vol. 6, pp. 14410–14430.

Akinci, B., Boukamp, F., Gordon, C., Huber, D., Lyons, C. and Park, K. (2006), “A formalism for utilization of sensor systems and integrated project models for active construction quality control”, *Automation in Construction,* Vol. 15 No. 2, pp. 124–138.

Alizadehsalehi, S. and Yitmen, I. (2019), “A Concept for Automated Construction Progress Monitoring: Technologies Adoption for Benchmarking Project Performance Control”, *The Arabian Journal for Science and Engineering (AJSE)*, Vol. 44 No. 5, pp. 4993–5008.

Alves, T. and Shah, N. (2018), "Analysis of Construction Contracts: Searching for Collaboration", *In the Proceedings of Construction Research Congress*, pp.148–57.

Bosché, F. (2010), “Automated recognition of 3D CAD model objects in laser scans and calculation of as-built dimensions for dimensional compliance control in construction”, *Advanced Enginnering Informatics*, Vol. 24 No. 1, pp. 107–118.

Braun, A. and Borrmann, A. (2019), “Combining inverse photogrammetry and BIM for automated labeling of construction site images for machine learning”, *Automation in Construction*, Vol. 106, pp. 102879.

Brilakis, I. and Soibelman, L. (2005), “Content-based search engines for construction image databases”, *Automation in Construction*, Vol. 14 No. 4, pp. 537–550.

Brilakis, I., Lourakis, M., Sacks, R., Savarese, S., Christodoulou, S., Teizer, J., and Makhmalbaf, A. (2010), “Toward automated generation of parametric BIMs based on hybrid video and laser scanning data”, *Advanced Engineering Informatics*, Vol. 24 No. 4, pp. 456–465.

Bull, D. (2014), “Digital Picture Formats and Representations”, *Communicating Pictures*, pp. 99–132.

Cai, B., Xu, X., Guo, K., Jia, K., Hu, B. and Tao, D. (2017), "A joint intrinsic-extrinsic prior model for Retinex", *IEEE International Conference on Computer Vision (ICCV)*, pp. 4020-4029.

Chang Y.-C. and Reid, J. F., (1996), “RGB calibration for color image analysis in machine vision”, *IEEE Transactions on Image Processing*, Vol. 5 No. 10, pp. 1414–1422.

Civil, C. I. N. (1993), “Computing in Civil and Building Engineering”, *Computing in Civil and Building Engineering,* pp. 955–1865.

Coleman, T.F. and Y. Li, (1996), “A reflective Newton method for minimizing a quadratic function subject to bounds on some of the aariables”, *Society for Industrial and Applied Mathematics (SIAM) Journal on Optimization*, Vol. 6 No.4, pp 1040–1058.

Deng, H., Hong, H., Luo, D., Deng, Y. and Su, C. (2020), “Automatic Indoor Construction Process Monitoring for Tiles Based on BIM and Computer Vision”, *Journal of Construction Engineering and Management,* Vol. 146 No. 1, pp. 04019095.

Dimitrov, A. and Golparvar-Fard, M. (2014), “Vision-based material recognition for automated monitoring of construction progress and generating building information modeling from unordered site image collections”, *Advanced Engineering Informatics*, Vol.28 No.1, pp. 37–49.

Dufaux. F, (2021), “Grand Challenges in Image Processing”, *Frontiers in Signal Processing*, Vol. 1, pp. 675547.

Ekanayake, B., Wong, J. K-W., Fini, A. A. F., and Smith, P. (2021), "Computer vision-based interior construction progress monitoring: A literature review and future research directions”, *Automation in Construction*, Vol. 127, pp.103705.

Elad, M., Matalon, B. and Zibulevsky, M. (2007), “Coordinate and subspace optimization methods for linear least squares with non-quadratic regularization”, *Applied and Computational Harmonic Analysis*, Vol. 23 No. 3, pp. 346–367.

Ergen, E., Akinci, B. and Sacks, R. (2007), “Tracking and locating components in a precast storage yard utilizing radio frequency identification technology and GPS”, *Automation in Construction*, Vol. 16 No. 3, pp. 354–367.

Fallis, A. (2013), "Towards the adoption of DevOps in software product organizations: A maturity model approach", *Journal of Chemical Information and Modeling,* Vol. 53 No.

9, pp. 1689–1699.

Fard, M. G.and Peña-Mora, F. (2007), “Application of visualization techniques for construction progress monitoring”, *In the Proceedings of ASCE International Workshop on Computing in Civil Engineering*, pp. 216–223.

Farid, H. (2001), “Blind inverse gamma correction”, *IEEE Transactions on Image Processing*, Vol. 10 No. 10, pp. 1428–1433.

Fathi, H., and Brilakis, I. (2012), “Machine vision-based infrastructure as-built documentation using edge points”, *Construction Research Congress*, pp. 757–766.

Fetic, A., Juric, D. and Osmankovic, D. (2012), "The procedure of a camera calibration using camera calibration toolbox for MATLAB", *In the Proceedings of 35th International Convention MIPRO*, pp. 1752-1757.

Franco-Duran D. M. and Guillermo M. G. (2016), “Assessing Cost Forecasting Performance in Construction Projects through Data Envelopment Analysis", *In the Proceeding of Construction Research Congress,* pp. 2039–2049.

Fu, H., Ma, H. and Wu, S. (2012), “Night removal by color estimation and sparse representation”, *In the 21st International Conference on Pattern Recognition (ICPR)*, pp. 11–15.

Fu, X., Zeng, D., Huang, Y., Liao, Y., Ding, X. and Paisley, J. (2016). “A fusion-based enhancing method for weakly illuminated images”, *Signal Processing*. Vol. 129, pp. 82–96.

Girshick, R., Donahue, J., Darrell, T. and Malik, J. (2014), “Rich feature hierarchies for accurate object detection and semantic segmentation”, *In the Proceedings of IEEE Computer Society Conference on Computer Vision and Pattern Recognition*, pp. 580-587.

Golparvar-Fard, M., Peña-Mora, F. and Savarese, S. (2015), “Automated progress monitoring using unordered daily construction photographs and IFC-based Building Information Models”, *Journal of Computing in Civil Engineering*, Vol. 29 No. 1, pp. 04014025.

Golparvar-Fard, M.; Peña-Mora, F.; Savarese, S. (2019), “Application of D4AR–a 4-dimensional augmented reality model for automating construction progress monitoring data collection, processing and communication”, *The Journal of Information*

Technology in Construction, Vol.14, pp.129–153.

Golparvar-Fard, M., Bohn, J., Teizer, J., Savarese, S. and Peña-Mora, F. (2016), “Evaluation of image-based modeling and laser scanning accuracy for emerging automated performance monitoring techniques”, *Automation in Construction*, Vol. 20 No. 8, pp. 1143–1155.

Guo, X., Li, Y. and Ling, H. (2017), “LIME: Low-light image enhancement via illumination map estimation”, *IEEE Transactions on Image Processing,* Vol. 26 No. 2, pp. 982–993.

Gurevich U. and Sacks, R. (2014), “Examination of the effects of a KanBIM production control system on subcontractors’ task selections in interior works”, *Automation in Construction*, Vol. 37, pp. 81–87.

Hamledari, H. (2016), "InPRO: automated indoor construction progress monitoring using unmanned aerial vehicles," Dissertation for the degree of Master of Applied Science, Department of Civil Engineering, University of Toronto.

Hamledari, H., McCabe, B. and Davari, S. (2017), “Automated computer vision-based detection of components of under-construction indoor partitions”, *Automation in Construction*, Vol. 74, pp. 78–94.

Hildreth, C. (1957), “A quadratic programming procedure”, *Naval Research Logistics Quarterly*, Vol. 4 No. 1, pp. 79-85.

Hong, M., Wang, X., Razaviyayn, M. and Luo, Z.Q. (2017), “Iteration complexity analysis of block coordinate descent methods”, *Mathematical Programming*, Vol. 163 No. 1–2, pp. 85–114.

Huang, S-C., Cheng, F-C. and Chiu, Y-S. (2013), "Efficient contrast enhancement using adaptive gamma correction with weighting distribution", *IEEE Transactions on Image Processing*, Vol. 22 No. 3, pp.1032–1041.

Jiang, Y., Gong, X., Liu, D.,Cheng, Y., Fang, C., Shen, X., Yang, J., Zhou, P., and Wang, Z. (2019), “EnlightenGAN: Deep light enhancement without paired supervision”, *arXiv*: 1906.06972

Kartika, I. and Mohamed, S. S. (2011), “Frame differencing with post-processing techniques for moving object detection in outdoor environment”, *In the Proceedings of IEEE 7th International Colloquium on Signal Processing and Its Applications*, pp. 172–176.

Kopsida, M., Brilakis, I. and Vela, P. (2015), "A Review of Automated Construction Progress and Inspection Methods", *In the Proceedings of 32nd CIB W78 Conference on Construction IT,* 27-29 October , Eindhoven, The Netherlands, pp. 421–431.

Kropp, C., Koch, C., König, M. and Brilakis, I. (2012), "A framework for automated delay prediction of finishing works using video data and BIM-based construction simulation", *In the Proceedings of 14th International Conference on Computing in Civil and Building Engineering (ICCCBE),* January, pp. 10–12.

Kropp, C., König, M., & Koch, C. (2013), "Object recognition in bim registered videos for indoor progress monitoring", *EG-ICE International Workshop on Intelligent Computing in Engineering*, pp. 1-10.

Kropp, C., Koch, C., & König, M. (2014), "Drywall state detection in image data for automatic indoor progress monitoring", *International Conference on Computing in Civil and Building Engineering*, pp. 347-354.

Kropp, C., Koch, C. and König, M. (2016), "Model-based pose estimation for visual indoor progress monitoring using line features", *In the Proceedings of the 16th International Conference on Computing in Civil and Building Engineering (ICCCBE2016)*, pp. 1–8.

Kropp, C., Koch, C. and König, M. (2017), "Interior construction state recognition with 4D BIM registered image sequences", *Automation in Construction*, Vol. 86, pp. 11–32.

Land, E. H. (1977), "The Retinex theory of color vision", *Scientific American*, Vol. 237 No. 6, pp. 108–129.

Li, J., Li, J., Fang, F., Li, F. and Zhang, G. (2020), "Luminance-aware pyramid network for low-light image enhancement", *IEEE Transactions on Multimedia*, Vol. 23, pp. 3153-3165.

Li, M., Liu, J., Yang, W., Sun, X. and Guo, Z. (2018), "Structure-revealing low-light image enhancement via robust Retinex model", *IEEE Transactions on Image Processing*, Vol. 27 No. 6, pp. 2828-2841.

Loh, Y. P., Liang, X. and Chan, C. S. (2019), "Low-light image enhancement using Gaussian Process for features retrieval", *Signal Processing: Image Communication*, Vol. 74, pp.175-190.

Łoza, A., Bull, D. R., Hill, P. R. and Achim, A. M. (2013), "Automatic contrast enhancement of low-light images based on local statistics of wavelet coefficients", *Digital Signal Processing*, Vol. 23 No. 6, pp. 1856–1866.

Lu, Q. and Lee, S. (2017), "Image-based technologies for constructing as-is Building Information Models for existing buildings", *Journal of Computing in Civil Engineering*, Vol. 31 No. 4, pp. 04017005.

Lukins, T. C. and Trucco, E. (2007), "Towards automated visual assessment of progress in construction projects", *Proceedings of the British Machine Conference,* BMVA Press, September, pp.18.1-18.10.

McCabe, B., Hamledari, H., Shahi, A., Zangeneh, P. andAzar, E.R. (2017), "Roles, benefits, and challenges of using UAVs for indoor smart construction applications", *In the Proceedings of the Computing in Civil Engineering,* pp. 349-357.

Memarzadeh, M., Golparvar-Fard, M. and Niebles, J. C. (2013), "Automated 2D detection of construction equipment and workers from site video streams using histograms of oriented gradients and colors", *Automation in Construction*, Vol. 32, pp. 24–37.

Omar T. and Nehdi, M. L. (2016), "Data acquisition technologies for construction progress tracking", *Automation in Construction*, Vol. 70, pp. 143–155.

Oneata, D., Revaud, J., Verbeek, J. and Schmid C. (2014), "Spatio-temporal object detection proposals", *In the European Conference on Computer Vision,* September, pp. 737–752.

Park, M. W. and Brilakis, I. (2012a), "Enhancement of construction equipment detection in video frames by combining with tracking," *In the Proceedings of the Congress on Computing in Civil Engineering*, June, pp. 421–428.

Park, M. W. and Brilakis, I. (2012b), "Construction worker detection in video frames for initializing vision trackers", *Automation in Construction*, Vol. 28, pp. 15–25.

Park, M.-W., Koch, C. and Brilakis, I. (2012), "Three-dimensional tracking of construction resources using an on-site camera system", *Journal of Computing in Civil Engineering*, Vol. 26 No. 4, pp. 541–549.

Percoco, G., Guerra, M.G., Sanchez Salmeron, A.J. and Galantucci, L.M. (2017), "Experimental investigation on camera calibration for 3D photogrammetric scanning of micro-features for micrometric resolution", *The International Journal of Advanced Manufacturing Technology,* Vol. 91 No. 9–12, pp. 2935–2947.

Poynton, C. A. (1993), "Gamma and its disguises: the nonlinear mappings of intensity in perception, CRTs, film, and video", *Society of Motion Picture and Television Engineers (SMPTE) Journal*, Vol. 102, pp. 1099–1108.

Rahmani, A., Ji, M., Mesbahi, M. and Egerstedt, M. (2009), “Controllability of multi-agent systems from a graph-theoretic perspective", *Society*, Vol. 48 No. 1, pp. 162–186.

Razavi, S.N., Young D., Nasir, H., Haas, C., Caldas, C. and Goodrum, P. (2008), "Field trial of automated material tracking in construction", *In the Proceedings of the Annual Conference of the Canadian Society for Civil Engineering,* CSCE, Quebec, Canada, pp. 1503–1511.

Ren, X., Li, M., Cheng, W. H., and Liu, J. (2018), "Joint enhancement and denoising method via sequential decomposition", *IEEE International Symposium on Circuits and Systems* (ISCAS), pp. 1-5.

Richez, J. (1963), “A trace following device", *Nuclear Instruments and Methods,* Vol. 20, pp. 419–421.

Saxena. D, and Cao. J, (2021), “Generative adversarial networks (GANs): challenges, solutions, and future directions”, ACM Computing Surveys (CSUR).

Shahi, A., Cardona, J. M., Haas, C. T., West, J. S. and Caldwell, G. L. (2012), “Activity-based data fusion for automated progress tracking of construction projects", *In the Proceedings of the Construction Research Congress: Construction Challenges in a Flat World,* pp. 838–847.

Shahi, A., Safa, M., Haas, C. T. and West, J. S. (2015), “Data fusion process management for automated construction progress estimation", *Journal of Computing in Civil Engineering,* Vol. 29 No. 6, pp. 04014098.

Teizer, J. (2015), “Status quo and open challenges in vision-based sensing and tracking of temporary resources on infrastructure construction sites”, *Advanced Engineering Informatics,* Vol. 29 Vo. 2, pp. 225–238.

Wang, J., Yang, Y., Chen, Y., and Han, Y. (2021), "LighterGAN: An Illumination Enhancement Method for Urban UAV Imagery", *Remote Sensoring.* Vol. 13, pp. 1371.

Wang, R., Zhang, Q., Fu, C.-W., Shen, X., Zheng, W.-S. and Jia, J. (2019), "Underexposed photo enhancement using deep illumination estimation", *In the Proceedings of*

IEEE/CVF Conference on Computer Vision and Pattern Recognition (CVPR), pp. 6842-6850.

Wang, Z., Bovik, A. C., Sheikh, H. R. and Simoncelli E. P. (2004), "Image quality assessment: from error visibility to structural similarity", *IEEE Transactions on Image Processing,* Vol. 13 No. 4, pp. 600-612.

Wright, S. J. (2015), “Coordinate descent algorithms”, *Mathematical Programming*, Vol. 151 No. 1, pp. 3–34.

Wu. C. (2011), "VisualSFM: A visual structure from motion system", accessed 20 July 2021, available from: http: //ccwu.me/vsfm/.

Wu, X. (2011), “A linear programming approach for optimal contrast-tone mapping”, *IEEE Transactions on Image Processing,* Vol. 20 No. 5, pp. 1262–1272.

Wu, C. and Xu, Y. (2020), "Greedy coordinate descent method on non-negative quadratic programming", IEEE 11th Sensor Array and Multichannel Signal Processing Workshop (SAM), pp. 1-5.

Xu, G., Su, J., Pan, H., Zhang, Z. and Gong, H. (2009), “An image enhancement method based on gamma correction", *In the Proceedings of Second International Symposium on Computational Intelligence and Design,* Vol. 1, pp. 60–63.

Xue, J., Hou, X., and Zeng, Y. (2021), “Review of Image-Based 3D Reconstruction of Building for Automated Construction Progress Monitoring”, *Applied Sciences,* Vol. 11, pp. 7840.

Yang, J., Park, M. W., Vela P. A. and Golparvar-Fard, M. (2015), “Construction performance monitoring via still images, time-lapse photos, and video streams: Now, tomorrow, and the future", *Advanced Enginnering Informatics*, Vol. 29 No. 2, pp. 211–224.

Ying, Z., Li, G. and Gao, W. (2015), ‘‘A bio-inspired multi-exposure fusion framework for low-light image enhancement", *Journal of Latex Class Files,* Vol. 14 No. 8, pp.1–10.

Zhang, X., Bakis, N., Lukins, T. C., Ibrahim, Y. M., Wu, S., Kagioglou, M., Aouad, G., Kaka, A. P. and Trucco, E. (2009), “Automating progress measurement of construction projects”, *Automation in Construction*, Vol. 18 No. 3, pp. 294-301.